mAbs 7:1, 96–109; January/February 2015; Published with license by Taylor & Francis Group, LLC

High contrast tumor imaging with radio-labeled antibody Fab fragments tailored for optimized pharmacokinetics via PASylation

Claudia T Mendler[1,2], Lars Friedrich[1], Iina Laitinen[2], Martin Schlapschy[1], Markus Schwaiger[2], Hans-Jürgen Wester[3], and Arne Skerra[1,4,*]

[1]Munich Center for Integrated Protein Science (CIPS-M) and Lehrstuhl für Biologische Chemie; Technische Universität München; Freising-Weihenstephan, Germany; [2]Nuklearmedizinische Klinik und Poliklinik; Klinikum rechts der Isar; Technische Universität München; München, Germany; [3]Lehrstuhl für Pharmazeutische Radiochemie; Technische Universität München; Garching, Germany; [4]XL-protein GmbH; Freising, Germany

Keywords: antibody fragment, CD20, HER2, PEGylation, plasma half-life, protein tracer

Abbreviations: ABD, albumin binding domain; CDC, complement-dependent cytotoxicity; CDR, complementarity-determining region; CLL, chronic lymphocytic leukemia; DMEM, Dulbecco's modified Eagle medium; EPR, enhanced permeability and retention effect; Fab, antigen-binding fragment; FACS, fluorescence-activated cell sorting; FBS, fetal bovine serum; FcRn, neonatal Fc receptor; HER2, human epidermal growth factor receptor 2; ID, injected dose; IDA, iminodiacetic acid; Ig, immunoglobulin; mAb, monoclonal antibody; MIP, maximum intensity projection; NHL, non-Hodgkin lymphoma; PET, positron emission tomography; p.i., post injection; PK, pharmacokinetics; RIT, radioimmuno therapy; scFv, single-chain variable antibody fragment; SEC, size exclusion chromatography; SPECT, single photon emission computed tomography; TLC, thin layer chromatography

Although antigen-binding fragments (Fabs) of antibodies constitute established tracers for in vivo radiodiagnostics, their functionality is hampered by a very short circulation half-life. PASylation, the genetic fusion with a long, conformationally disordered amino acid chain comprising Pro, Ala and Ser, provides a convenient way to expand protein size and, consequently, retard renal filtration. Humanized αHER2 and αCD20 Fabs were systematically fused with 100 to 600 PAS residues and produced in *E. coli*. Cytofluorimetric titration analysis on tumor cell lines confirmed that antigen-binding activities of the parental antibodies were retained. The radio-iodinated PASylated Fabs were studied by positron emission tomography (PET) imaging and biodistribution analysis in mouse tumor xenograft models. While the unmodified αHER2 and αCD20 Fabs showed weak tumor uptake (0.8% and 0.2% ID/g, respectively; 24 h p.i.) tumor-associated radioactivity was boosted with increasing PAS length (up to 9 and 26-fold, respectively), approaching an optimum for Fab-PAS_{400}. Remarkably, 6- and 5-fold higher tumor-to-blood ratios compared with the unmodified Fabs were measured in the biodistribution analysis (48 h p.i.) for αHER2 Fab-PAS_{100} and Fab-PAS_{200}, respectively. These findings were confirmed by PET studies, showing high imaging contrast in line with tumor-to-blood ratios of 12.2 and 5.7 (24 h p.i.) for αHER2 Fab-PAS_{100} and Fab-PAS_{200}. Even stronger tumor signals were obtained with the corresponding αCD20 Fabs, both in PET imaging and biodistribution analysis, with an uptake of 2.8% ID/g for Fab-PAS_{100} *vs*. 0.24% ID/g for the unmodified Fab. Hence, by engineering Fabs via PASylation, plasma half-life can be tailored to significantly improve tracer uptake and tumor contrast, thus optimally matching reagent/target interactions.

Introduction

Monoclonal antibodies (mAbs), including their antigen-binding fragments (Fabs), constitute the fastest growing class of biotherapeutic agents today.[1,2] Among those, in particular the "blockbuster" antibodies trastuzumab (Herceptin®) and rituximab (Rituxan®), which are directed against human epidermal growth factor receptor 2 (HER2) and the B-cell antigen CD20, respectively, are successfully applied for the treatment of tumors in patients with metastatic breast cancer and non-Hodgkin lymphoma (NHL).[3] Apart from such naked IgGs, radio-immunoconjugates like ^{90}Y ibritumomab tiuxetan (Zevalin®), also directed against CD20, have shown promise for tumor targeting in clinical therapy.[4]

HER2 is overexpressed in 20-30% of primary breast cancers,[5] but also in other tumor types, including ovarian, bladder, pancreatic and lung cancer, which is usually associated with poor prognosis.[6] In 1998 the US Food and Drug Administration (FDA) approved the humanized IgG1/κ trastuzumab – initially obtained by

*Correspondence to: Arne Skerra; Email: skerra@tum.de
Submitted: 08/24/2014; Revised: 10/15/2014; Accepted: 10/28/2014
http://dx.doi.org/10.4161/19420862.2014.985522

complementarity-determining region (CDR) grafting from the mouse mAb 4D5 and subsequently engineered toward improved affinity[7] – for the treatment of patients with HER2-positive metastatic breast cancer alone or in combination with chemotherapy.[8] Recently, the antibody-drug conjugate ado-trastuzumab emtansine (T-DM1, Kadcyla®), developed by chemical coupling of trastuzumab with the cytotoxin mertansine, was approved.[9]

CD20 is expressed on the pre-B to mature B-cell lineage and occurs in >90% of patients with B-cell lymphoma, whereas most plasma immune cells are CD20 negative.[10,11] The human IgG1/κ ofatumumab (2F2, Arzerra®), generated in human Ig-transgenic mice, was approved by the FDA in 2009 for patients with chronic lymphocytic leukemia (CLL).[12] The reduced immunogenicity of ofatumumab compared to the first CD20-targeting mAb to be approved, rituximab (Rituxan®/MabThera®), led to reduced side effects in clinical studies.[13] Its lower off-rate further contributed to more efficient complement-dependent cytotoxicity (CDC) on target cells compared to rituximab.[14]

Although several radio-labelled mAbs have been developed for cancer radioimmunotherapy (RIT) and evaluated in clinical trials during the last decades,[15] radioimmuno-imaging has attracted even greater attention for target evaluation and dosimetry. Recently, immuno-positron emission tomography (Immuno-PET) has gained particular interest since long-lived positron emitters such as ^{124}I and ^{89}Zr have become commercially available.[16] For example, ^{89}Zr-trastuzumab was applied to non-invasively assess the HER2 status in patients with metastatic breast cancer.[17,18] In another study, the chimeric IgG1/κ antibody ^{124}I-cG250 directed against carbonic anhydrase IX was used to diagnose clear-cell renal carcinoma in 26 patients.[19]

Due to their intrinsically long plasma half-life, typically in the range of 2-3 weeks,[20] which allows extended contact time with cell surface antigens, and also owing to the enhanced permeability and retention effect (EPR),[21,22] full-size antibodies can reach high uptake levels in tumor tissue. On the other hand, their poor tissue penetration and often inhomogeneous distribution, which leaves areas of the tumor untargeted, is a general problem for tumor therapy[23] as well as high-precision imaging. Furthermore, the prolonged circulation time leads to high background in the blood, especially at shorter time points, as well as exposure of healthy organs to the radionuclide conjugate, which often causes side effects and appears dose limiting in RIT.[24]

Especially for in vivo diagnostic applications, where high tumor imaging contrast (i.e., signal-to-background ratio) is desired shortly after tracer administration, antibody fragments with their better tissue penetration, much faster blood clearance and lack of FcRn binding, which is responsible for Fc-mediated endosomal recycling of full-size immunoglobulins (Igs), are preferred.[25,26] Conversely, their smaller size and very fast kidney clearance (from minutes to a few hours in humans) often prevents sufficient accumulation of the tracer at the targeted tumor tissue, and is responsible for the rapid wash-out at later time points when plasma concentrations are decreased.[25,27,28] Consequently, improving the targeting properties of antibody fragments by manipulating their plasma half-life via protein engineering may provide even more useful radioimaging reagents.

Up to now, several attempts were made to prolong the circulation and control the in vivo biodistribution of protein-based tracers. For example, fusion with a phage-derived albumin binding peptide has been employed to extend plasma half-life of the HER2-specific Fab 4D5, which indeed led to higher tumor accumulation.[27] This approach took advantage of the high abundance and intrinsically long life-time of serum albumin, which like IgGs possesses a size above the threshold for renal filtration and moreover gets recycled via FcRn.[29,30] However, as albumin is catabolized by many tumors,[31,32] which generally promotes tumor uptake of an associated tracer, it is difficult to ascribe the observed effects to the increased plasma half-life alone.

An alternative, clinically-approved method to retard renal clearance of bioactive proteins is the chemical conjugation with polyethylene glycol (PEG), which enlarges the hydrodynamic molecular volume beyond the glomerular pore size.[33] Previous studies have shown that PEGylation of a single-chain variable antibody fragment (scFv), and also of a designed ankyrin repeat protein (DARPin), both directed against HER2, led to enhanced tumor uptake.[34,35] However, the longer persistence in plasma due to the fusion with a 20 kDa PEG moiety also resulted in lower tumor-to-blood ratios.

Recently, PASylation technology was developed as a biological alternative to PEGylation.[36] In this case, a long biosynthetic polypeptide composed of the 3 small amino acids Pro, Ala and Ser (PAS), was designed to adopt a highly solvated random coil structure under physiological conditions with very similar biophysical properties as PEG, thus drastically increasing the hydrodynamic volume of the attached protein reagent. In this manner, much prolonged plasma half-life, depending on the length of the PAS sequence, can be achieved while, in contrast to PEG, PAS constitutes a biodegradable and non-immunogenic polymer. Another major advantage of PASylation is that the amino acid polymer can be genetically encoded and directly produced as a fusion protein, thus avoiding the laborious optimization of chemical coupling conditions.[37] Using premade gene cassettes, the precise tuning of the length of the PAS tag attached to a functional binding protein is easily achieved. Hence, the loss of binding activity, which often accompanies PEGylation of proteins, as well as the formation of a heterogeneous bioconjugate, is prevented.

In the present study, we have employed PASylation of recombinant Fab fragments with specific tumor-targeting activities to tailor their pharmacokinetic (PK) properties and investigated the effect on both tumor uptake and tumor-to-normal tissue or tumor-to-blood ratio. To this end, we utilized the αHER2 Fab derived from trastuzumab (hu4D5-v8)[7] and the αCD20 Fab derived from ofatumumab (2F2)[38] as model tracers with clinical relevance because both their antigens represent established tumor markers.[39] The two Fab fragments were fused to PAS sequences of 100 up to 600 residues and functionally produced in *E. coli*, followed by radio-iodination and PET imaging, as well as biodistribution analysis in CD1-*Foxn1*^{nu} mice bearing HER2- and CD20-positive tumor xenografts, respectively.

Results

Preparation of PASylated αHER2 and αCD20 Fabs with extended plasma half-life

For in vivo imaging of HER2-positive xenograft tumors, an affinity-matured version of the αHER2 Fab fragment based on trastuzumab was used. First, a couple of conservative amino acid exchanges at the N- and C-termini of the V-gene regions that had been inserted to facilitate cloning during construction of the previously described *E. coli* expression vector pASK88-4D5[40] were reversed by site-directed mutagenesis to fully match the hu4D5-v8 sequence.[7] Second, a single point mutation, $D^{H98}W$, which was described to result in threefold improved antigen affinity,[41] was introduced into CDR-H3.

For in vivo imaging of CD20-positive xenograft tumors, the recombinant Fab fragment 2F2 derived from ofatumumab[14] was cloned after gene synthesis of the V-gene regions by insertion into pASK88 in the same format as the αHER2 Fab. pASK88 provides for human IgG1/κ constant gene regions, with a His_6-tag attached to the C-terminus of the heavy chain as well as *E. coli* signal sequences to direct periplasmic secretion.[42]

To dissect the influence of circulation half-life on tumor uptake in mouse xenograft models, PAS sequences comprising 100, 200, 400 and 600 amino acid residues were fused to the C-terminus of the light chain according to a previously published strategy[36] (**Fig. 1**). For comparison, analogous fusion proteins of both Fabs with the *Streptococcal* albumin binding domain (ABD),[43] thus utilizing complex formation with serum albumin,[27] were constructed. The Fab of the murine mAb IN1 directed against the unrelated neuronal surface protein Nogo-A[44] served as a negative control.

All Fabs were produced as functional proteins in the periplasm of *E. coli*, where disulfide bond formation and light/heavy chain association can readily occur, and purified to homogeneity by means of His_6 and *Strep*-tag II affinity chromatography, size exclusion chromatography (SEC) and ion exchange chromatography. A protein yield of 0.4 mg l^{-1} OD^{-1} from shake flask culture was obtained for the αCD20 Fab, comparable to the 4D5 Fab,[40] while the affinity-matured version of the latter Fab showed slightly decreased yield (0.2 mg l^{-1} OD^{-1}). Notably, PASylation did not significantly affect protein yield.

Proper disulfide bridge formation, with ≥95% covalent linkage between light and heavy chains as well as a reduced electrophoretic mobility depending on the length of the attached PAS tag, was detected by SDS-PAGE analysis. These results were consistent with a previous report on protein PASylation.[36] Likewise, SEC analysis revealed a homogeneous peak with decreasing elution volume upon increasing PAS length, indicating an expanded molecular size and a much enlarged hydrodynamic volume of the PASylated Fabs, as expected.

To assess binding activity towards the corresponding tumor antigens, fluorescence-activated cell sorting (FACS) titration analyses were performed on the HER2- and CD20-positive human tumor cell lines SK-BR-3[45] and Granta,[46] respectively. While the affinity-matured αHER2 Fab showed a dissociation constant of 2.2 nM, a K_D value of 8.0 nM was measured for the αCD20 Fab (**Fig. 1**). Neither PASylation nor fusion with the ABD had a strong influence on this functional binding activity, which was even less than the small reduction in affinity observed during surface plasmon resonance measurements before.[36] The same was the case for non-radioactive iodination of the αHER2 Fab. Overall, the measured affinities were comparable to those of the parental antibodies trastuzumab and ofatumumab, for which K_D values of around 5 nM had been reported on the basis of in vitro cell assays.[47,48]

For subsequent in vivo tumor imaging, the αHER2 and αCD20 Fabs as well as their fusion proteins were radiolabeled via the Iodogen coupling procedure[49] with the β^+/γ emitter ^{124}I, whereas the γ emitter ^{125}I was chosen for in vivo biodistribution analysis. In addition, ^{125}I was used in combination with ^{124}I or with the γ emitter ^{123}I for dual tracer experiments.

In vivo PET tumor imaging

To evaluate the PK and biodistribution properties of the radio-iodinated αHER2 and αCD20 Fabs in their various PASylated formats, in vivo PET imaging was performed using CD1-*Foxn1^{nu}* mice bearing HER2- or CD20-positive human tumor

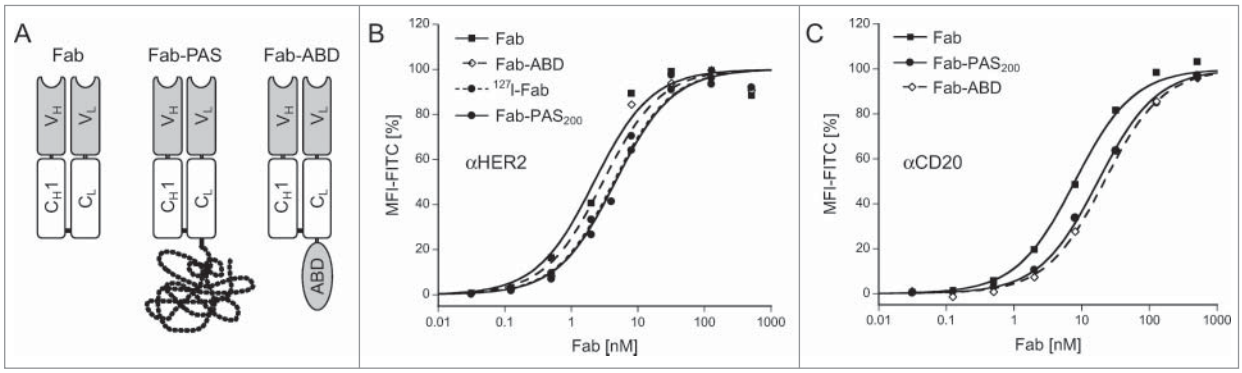

Figure 1. In vitro characterization of purified recombinant Fabs. (**A**) Schematic representation of the bacterially produced Fab format and its fusions with a PAS polypeptide or an albumin binding domain (ABD). (**B, C**) FACS titration analyses of αHER2 and αCD20 Fabs in different formats *versus* corresponding tumor cell lines. Fabs were incubated with SK-BR-3 (HER2) or Granta (CD20) cells for 1 h at 4°C and, after washing, bound Fab was detected with a fluorescein-conjugated αhu-kappa-light chain antibody. Hyperbolic curve fit (see Materials and Methods) revealed K_D values of 2.2 ± 0.6 nM for αHER2 Fab, 4.6 ± 0.9 nM for αHER2 Fab-PAS_{200}, 3.0 ± 0.7 nM for αHER2 Fab-ABD, 4.3 ± 0.6 nM for the (non-radioactively) iodinated αHER2 Fab as well as 8.0 ± 1.1 nM for αCD20 Fab, 15.6 ± 5.7 nM for αCD20 Fab-ABD and 17.5 ± 1.0 nM for αCD20 Fab-PAS_{200}.

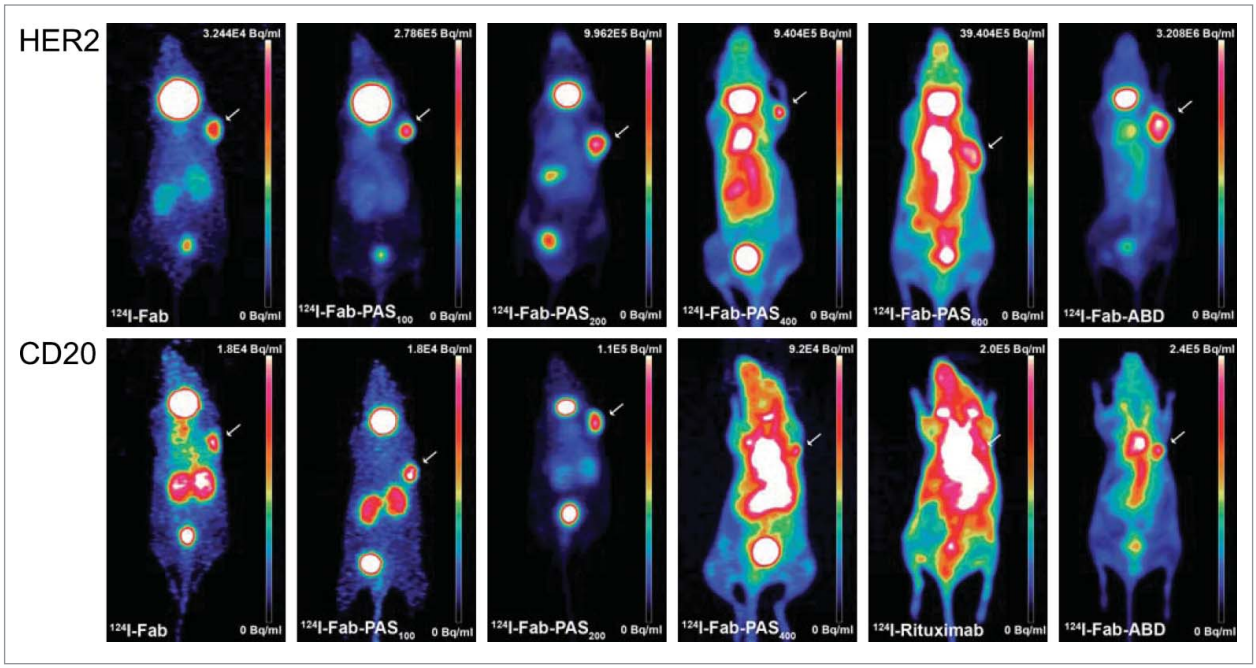

Figure 2. MIP-PET images of xenograft tumors in mice using ^{124}I-labeled αHER2 and αCD20 Fab fragments, respectively. CD1-*Foxn1*^{nu} mice bearing s.c. HER2-positive (SK-BR-3) or CD20-positive (Granta) xenografts at the right shoulder (see arrows) were injected with ^{124}I-labeled recombinant Fabs in different molecular formats: Fab, Fab-PAS$_{100}$, Fab-PAS$_{200}$, Fab-PAS$_{400}$, Fab-PAS$_{600}$, Fab-ABD as well as, for comparison, the full-size IgG rituximab. PET scans were performed 24 h p.i. for HER2 (top) and CD20 (bottom). Regardless of the reagent used, the thyroid gave rise to elevated background signals in all mice because this organ was not blocked for iodine uptake in these experiments.

xenografts. For comparison of the different constructs, PET images corresponding to representative static maximum intensity projections (MIP) were collected 24 h p.i. (**Fig. 2**), when a high tumor-to-background ratio was reached. At this time point, both unmodified Fabs allowed visualization of the tumor.

Notably, the αHER2 Fab fragment led to a better tumor-to-background ratio and lower kidney accumulation, possibly due to its higher target affinity. A moderate radioactive signal in the bladder indicated renal excretion of both ^{124}I-Fabs, as expected for proteins smaller than the glomerular pore size. The observed considerable thyroid accumulation was likely due to dehalogenation of the tracer, as iodide uptake by this organ was not specifically blocked.[50] Iodide is also transported from the bloodstream into the gastric lumen,[51] as was detectable via stomach uptake of radioactivity for some of the constructs.

Apart from this general pattern, which is in line with previous in vivo imaging and biodistribution studies of radio-iodinated Fabs,[52] there was a strong effect on the signal distribution upon applying PASylation, corresponding to an extension of (murine) plasma half-life in the range from approximately 1.3 (for the unfused Fab) to 28 h (in the case of the PAS$_{600}$ tag).[36] In particular, PASylation led to a much enhanced imaging contrast 24 h p.i. for Fab-PAS$_{100}$ and Fab-PAS$_{200}$ compared with the unmodified Fabs, both for the HER2 and CD20 target (**Fig. 2**). This effect was particularly evident for the αCD20 Fab, where the fusion with 200 PAS residues led to comparable high tumor-to-background ratio as for the αHER2 Fab-PAS$_{200}$ in spite of its lower target affinity, as noted above.

In contrast, investigation of the Fabs carrying longer PAS sequences of 400 or 600 residues revealed an increasing background signal 24 h p.i. which was mainly detectable for the highly perfused organs, eventually leading to a lower tumor-to-normal tissue ratio. In fact, for the long PAS tags the biodistribution pattern approached that of full-length antibodies, such as ^{124}I-rituximab (**Fig. 2**), with a typically poor tumor-to-blood ratio of 0.5 at 24 h p.i., which is in agreement with published data.[53]

Notably, fusion of the αCD20 and αHER2 Fabs with the ABD, as an alternative strategy to prolong circulation via association with albumin,[27] also resulted in good imaging contrast 24 h p.i. Compared with the structurally more expanded Fab-PAS$_{600}$ construct, which has similar plasma half-life,[36] the tumor-to-normal tissue ratio was actually better. However, albumin binding resulted in unfavorable accumulation of radioactivity in the blood, especially for the αCD20 Fab-ABD construct (cf. **Fig. 2** and **Table 2**). Thus, the highly perfused organs like heart and lung became strongly visible, resulting in much poorer imaging contrast for the ABD fusion than for the PAS$_{100/200}$ versions described above.

Biodistribution of radiolabeled αHER2 and αCD20 Fabs

In vivo biodistribution studies were performed using the same subcutaneous human tumor xenograft models. Mice were injected with 5 pmol (specific activity 80–100 MBq/nmol) of the radio-iodinated Fabs. At 24 h p.i., both unmodified Fabs showed specific but rather low tumor accumulation of 0.80% ID/g for HER2-positive and 0.24% ID/g for CD20-positive xenografts (**Tables 1 and 2**). Nevertheless, a respectable tumor-to-blood

Table 1. Biodistribution of radio-iodinated αHER2 Fabs (for tumor-to-organ ratios see **Fig. S1**)

	^{125}I-Fab			^{125}I-Fab-PAS$_{100}$*			^{125}I-Fab-PAS$_{200}$*		
[%ID/g]	**6 h**	**24 h**	**48 h**	**6 h**	**24 h**	**48 h**	**6 h**	**24 h**	**48 h**
Tumor	2.67 ± 0.33	0.80 ± 0.32	0.33 ± 0.15	7.41 ± 1.02	2.69 ± 1.05	1.20 ± 0.43	3.40 ± 0.70	2.15 ± 0.95	2.77 ± 0.79
Blood	2.46 ± 0.47	0.15 ± 0.02	0.13 ± 0.03	4.10 ± 0.39	0.22 ± 0.10	0.08 ± 0.04	4.16 ± 0.82	0.38 ± 0.11	0.24 ± 0.03
Heart	0.91 ± 0.17	0.06 ± 0.01	0.06 ± 0.02	1.49 ± 0.12	0.10 ± 0.05	0.04 ± 0.01	1.24 ± 0.13	0.11 ± 0.04	0.08 ± 0.01
Lung	1.76 ± 0.34	0.16 ± 0.07	0.14 ± 0.08	2.90 ± 0.34	0.25 ± 0.09	0.10 ± 0.03	2.18 ± 0.33	0.25 ± 0.08	0.17 ± 0.02
Liver	0.96 ± 0.19	0.09 ± 0.02	0.12 ± 0.04	1.14 ± 0.13	0.11 ± 0.04	0.07 ± 0.03	1.04 ± 0.22	0.10 ± 0.02	0.08 ± 0.01
Spleen	1.73 ± 0.52	0.06 ± 0.01	0.05 ± 0.01	1.96 ± 0.41	0.17 ± 0.09	0.05 ± 0.01	1.18 ± 0.18	0.10 ± 0.03	0.11 ± 0.03
Kidney	2.34 ± 0.36	0.21 ± 0.03	0.16 ± 0.03	8.39 ± 1.19	0.35 ± 0.08	0.12 ± 0.02	3.09 ± 0.49	0.27 ± 0.07	0.23 ± 0.02
A. gland	0.83 ± 0.21	0.09 ± 0.03	0.14 ± 0.07	1.62 ± 0.35	0.29 ± 0.12	0.07 ± 0.02	1.63 ± 0.39	0.10 ± 0.02	0.16 ± 0.02
Pancreas	1.56 ± 0.26	0.04 ± 0.01	0.04 ± 0.01	2.11 ± 0.70	0.13 ± 0.07	0.03 ± 0.02	0.93 ± 0.14	0.07 ± 0.02	0.06 ± 0.01
Stomach	10.03 ± 1.70	0.21 ± 0.07	0.13 ± 0.04	10.67 ± 3.89	0.59 ± 0.31	0.10 ± 0.05	3.25 ± 0.80	0.21 ± 0.08	0.16 ± 0.07
S. int.	1.93 ± 0.36	0.09 ± 0.02	0.11 ± 0.07	2.12 ± 0.33	0.20 ± 0.09	0.05 ± 0.03	0.83 ± 0.14	0.07 ± 0.03	0.07 ± 0.02
L. int.	2.13 ± 0.54	0.11 ± 0.05	0.12 ± 0.04	2.51 ± 0.64	0.26 ± 0.20	0.06 ± 0.04	0.55 ± 0.11	0.06 ± 0.01	0.07 ± 0.01
Muscle	0.46 ± 0.09	0.02 ± 0.00	0.02 ± 0.01	0.75 ± 0.21	0.05 ± 0.02	0.03 ± 0.04	0.35 ± 0.03	0.04 ± 0.01	0.03 ± 0.01
Bone	0.76 ± 0.16	0.03 ± 0.01	0.03 ± 0.01	0.88 ± 0.13	0.08 ± 0.03	0.03 ± 0.01	0.57 ± 0.09	0.05 ± 0.01	0.04 ± 0.01
Skin	1.86 ± 0.45	0.14 ± 0.03	0.10 ± 0.04	2.69 ± 0.81	0.25 ± 0.09	0.06 ± 0.01	1.30 ± 0.18	0.15 ± 0.05	0.12 ± 0.02
Brain [% ID]	0.13 ± 0.02	0.01 ± 0.00	0.02 ± 0.01	0.15 ± 0.01	0.02 ± 0.00	0.01 ± 0.01	0.13 ± 0.02	0.01 ± 0.00	0.01 ± 0.00
Thyroid	5.28 ± 3.06	8.47 ± 4.33	3.34 ± 1.40	6.72 ± 3.11	6.30 ± 2.71	8.53 ± 1.35	0.74 ± 0.22	2.56 ± 0.81	4.26 ± 1.49
	^{123}I-Fab-PAS$_{400}$*			^{124}I-Fab-PAS$_{600}$*			^{125}I-Fab-ABD		
[%ID/g]	**6 h**	**24 h**	**48 h**	**6 h**	**24 h**	**48 h**	**6 h**	**24 h**	**48 h**
Tumor	6.64 ± 0.59	7.19 ± 2.22	5.30 ± 1.01	4.61 ± 1.31	5.77 ± 0.94	3.72 ± 0.37	10.79 ± 2.07	15.42 ± 5.63	12.41 ± 3.19
Blood	18.46 ± 1.63	7.31 ± 0.94	2.06 ± 0.66	17.39 ± 4.35	8.22 ± 0.56	4.16 ± 0.63	21.17 ± 4.17	9.86 ± 2.85	5.75 ± 1.34
Heart	5.56 ± 0.89	1.98 ± 0.39	0.52 ± 0.15	4.24 ± 1.08	1.87 ± 0.36	0.98 ± 0.10	6.97 ± 1.73	3.16 ± 1.06	1.79 ± 0.34
Lung	7.32 ± 1.04	2.90 ± 0.45	1.05 ± 0.21	7.10 ± 2.16	2.90 ± 0.33	1.53 ± 0.23	10.33 ± 2.28	4.90 ± 1.96	2.74 ± 0.73
Liver	4.45 ± 0.67	1.64 ± 0.09	0.61 ± 0.10	3.55 ± 1.09	1.51 ± 0.14	0.99 ± 0.13	4.53 ± 0.60	2.01 ± 0.62	1.14 ± 0.24
Spleen	2.72 ± 0.20	1.46 ± 0.28	0.62 ± 0.13	2.60 ± 0.79	1.18 ± 0.30	1.19 ± 0.21	3.64 ± 0.86	1.55 ± 0.54	0.95 ± 0.17
Kidney	7.53 ± 1.03	3.13 ± 0.29	0.85 ± 0.20	4.24 ± 1.26	1.91 ± 0.13	1.15 ± 0.25	4.76 ± 0.99	2.33 ± 0.71	1.32 ± 0.26
A. gland	3.73 ± 0.99	2.13 ± 0.34	0.42 ± 0.07	5.20 ± 1.76	2.19 ± 0.93	1.14 ± 0.32	4.10 ± 1.82	2.46 ± 0.81	1.11 ± 0.15
Pancreas	1.85 ± 0.47	1.16 ± 0.16	0.29 ± 0.09	1.62 ± 0.35	0.63 ± 0.10	0.41 ± 0.07	1.77 ± 0.54	1.14 ± 0.28	0.65 ± 0.12
Stomach	3.82 ± 0.82	2.30 ± 0.64	0.65 ± 0.19	3.07 ± 0.60	1.14 ± 0.13	0.79 ± 0.13	3.79 ± 0.75	1.57 ± 0.32	0.91 ± 0.14
S. int.	1.84 ± 0.21	1.03 ± 0.23	0.28 ± 0.07	1.48 ± 0.28	0.48 ± 0.06	0.40 ± 0.03	2.45 ± 0.36	1.04 ± 0.33	0.62 ± 0.13
L. int.	1.67 ± 0.36	1.05 ± 0.25	0.31 ± 0.06	0.91 ± 0.22	0.37 ± 0.08	0.34 ± 0.04	1.44 ± 0.33	0.67 ± 0.16	0.47 ± 0.11
Muscle	0.66 ± 0.20	0.48 ± 0.04	0.16 ± 0.07	0.55 ± 0.07	0.37 ± 0.08	0.23 ± 0.10	0.90 ± 0.25	0.74 ± 0.28	0.50 ± 0.09
Bone	1.39 ± 0.36	0.98 ± 0.18	0.20 ± 0.05	1.48 ± 0.30	0.66 ± 0.16	0.34 ± 0.06	1.82 ± 0.17	0.98 ± 0.38	0.54 ± 0.11
Skin	2.56 ± 0.97	1.64 ± 0.28	0.44 ± 0.08	2.28 ± 0.54	1.39 ± 0.08	0.81 ± 0.07	3.62 ± 0.87	2.48 ± 0.73	1.64 ± 0.26
Brain [% ID]	0.52 ± 0.06	0.22 ± 0.05	0.06 ± 0.02	0.47 ± 0.11	0.18 ± 0.04	0.12 ± 0.02	0.53 ± 0.07	0.21 ± 0.07	0.14 ± 0.02
Thyroid	1.16 ± 0.58	2.89 ± 1.49	6.08 ± 1.40	0.54 ± 0.22	2.07 ± 0.32	2.63 ± 0.82	0.19 ± 0.04	2.41 ± 0.97	2.20 ± 1.32

*Biodistribution was quantified in dual tracer experiments in the combinations ^{125}I-Fab-PAS$_{100}$ / ^{123}I-Fab-PAS$_{400}$ and ^{125}I-Fab-PAS$_{200}$ / ^{124}I-Fab-PAS$_{600}$.

ratio of 5.3 and 4.0 was detected for the αHER2 and αCD20 Fabs, respectively. As expected, no accumulation of the negative control Fab IN1 was observed for the SK-BR-3 xenograft (0.07% ID/g 24 h p.i.) (cf. **Fig. 3**).

Compared to the unmodified protein reagents, the series of different PASylated αHER2 and αCD20 Fabs with their successively extended plasma half-lives exhibited increasing tumor uptake with a maximum for 400 PAS residues: 7.2% ID/g for αHER2 and 6.3% ID/g for αCD20 24 h p.i. (**Tables 1 and 2; Fig. 3A**). Notably, the highest tumor accumulation with 15.4% ID/g for αHER2 and 12.3% ID/g for αCD20 was observed for the ^{125}I-Fab-ABD version 24 h p.i., yet at a relatively low tumor-to-blood ratio of 1.6, likely due to the association with albumin in the blood plasma. Again, dehalogenation of the radiotracer seemed responsible for generally high levels of radioactivity in thyroid and stomach, as evident in the biodistribution for Fab and Fab-PAS$_{100}$ 6 h p.i. (**Tables 1** and **2**). Possibly, PASylation with 200 or more amino acid residues as well as fusion with an ABD improved the in vivo stability of the Fab fragments, since, for these tracers, less of the iodine isotope could be detected in those organs.

In control experiments, CD1-*Foxn1^{nu}* mice bearing HER2-positive xenografts were treated with a 1,000-fold excess of trastuzumab before measuring target-specific accumulation of radio-iodinated Fab-ABD, Fab-PAS$_{200}$ and Fab-PAS$_{600}$ (**Fig. S3**). Under these conditions, biodistribution studies 24 h p.i. showed clearly reduced tumor uptake for ^{125}I-Fab-ABD, from 15.4% ID/g to 6.2% ID/g ($p < 0.05$). Likewise, the αHER2 Fab-PAS$_{200}$ and Fab-PAS$_{600}$ also yielded much lower tumor uptake after blocking with the antibody

Table 2. Biodistribution of radio-iodinated αCD20 Fabs (for tumor-to-organ ratios see **Fig. S2**)

	^{125}I-Fab*			^{125}I-Fab-PAS$_{100}$*			^{124}I-Fab-PAS$_{200}$*			^{124}I-Fab-PAS$_{400}$*			^{124}I-Fab-PAS$_{200}$	^{125}I-Fab-ABD
[%ID/g]	**6 h**	**24 h**	**48 h**	**6 h**	**24 h**	**48 h**	**6 h**	**24 h**	**48 h**	**6 h**	**24 h**	**48 h**	**Block 24 h**	**24 h**
Tumor	1.33 ± 0.14	0.24 ± 0.09	0.17 ± 0.07	8.45 ± 1.38	2.82 ± 0.58	2.18 ± 1.15	4.15 ± 1.21	2.41 ± 0.76	1.47 ± 0.67	4.03 ± 0.71	6.33 ± 1.73	2.92 ± 1.55	0.68 ± 0.38	12.29 ± 3.53
Blood	1.39 ± 0.37	0.06 ± 0.01	0.04 ± 0.01	6.98 ± 1.77	0.37 ± 0.08	0.26 ± 0.08	6.71 ± 0.65	0.59 ± 0.24	0.09 ± 0.02	15.63 ± 2.89	5.86 ± 0.52	1.58 ± 0.66	0.63 ± 0.11	11.52 ± 0.17
Heart	0.52 ± 0.18	0.03 ± 0.00	0.02 ± 0.00	2.58 ± 0.56	0.17 ± 0.05	0.12 ± 0.04	2.42 ± 0.49	0.19 ± 0.09	0.04 ± 0.00	4.98 ± 0.76	1.77 ± 0.20	0.50 ± 0.22	0.25 ± 0.09	3.54 ± 0.45
Lung	1.16 ± 0.43	0.08 ± 0.04	0.06 ± 0.02	5.11 ± 0.94	0.44 ± 0.13	0.35 ± 0.12	3.82 ± 0.71	0.43 ± 0.18	0.14 ± 0.09	6.98 ± 0.46	2.43 ± 0.08	0.71 ± 0.28	0.47 ± 0.16	5.36 ± 0.41
Liver	0.52 ± 0.12	0.04 ± 0.01	0.04 ± 0.01	2.44 ± 0.56	0.21 ± 0.06	0.26 ± 0.09	1.62 ± 0.16	0.18 ± 0.06	0.06 ± 0.01	3.18 ± 0.48	1.10 ± 0.11	0.35 ± 0.10	0.21 ± 0.03	2.03 ± 0.08
Spleen	0.97 ± 0.54	0.04 ± 0.01	0.03 ± 0.01	3.77 ± 0.36	0.22 ± 0.06	0.20 ± 0.08	2.02 ± 0.51	0.25 ± 0.06	0.08 ± 0.02	2.63 ± 0.46	1.00 ± 0.15	0.42 ± 0.15	0.26 ± 0.08	1.65 ± 0.13
Kidney	2.75 ± 0.51	0.41 ± 0.07	0.23 ± 0.04	19.39 ± 1.78	0.86 ± 0.23	0.56 ± 0.19	13.40 ± 2.33	0.92 ± 0.33	0.17 ± 0.03	11.15 ± 2.44	2.62 ± 0.25	0.83 ± 0.30	1.10 ± 0.33	2.63 ± 0.32
A. gland	0.73 ± 0.42	0.04 ± 0.02	0.04 ± 0.01	4.38 ± 1.09	0.45 ± 0.15	0.27 ± 0.16	3.46 ± 1.20	0.37 ± 0.12	0.11 ± 0.03	5.78 ± 1.97	2.67 ± 0.63	0.58 ± 0.18	0.98 ± 1.37	2.75 ± 0.47
Pancreas	1.10 ± 0.44	0.02 ± 0.01	0.01 ± 0.00	4.92 ± 0.68	0.17 ± 0.05	0.09 ± 0.04	1.89 ± 0.20	0.19 ± 0.07	0.03 ± 0.01	2.02 ± 0.25	0.76 ± 0.09	0.18 ± 0.11	0.14 ± 0.02	1.31 ± 0.17
Stomach	6.02 ± 3.11	0.10 ± 0.04	0.04 ± 0.01	15.47 ± 6.09	0.62 ± 0.10	0.27 ± 0.17	6.53 ± 2.87	0.59 ± 0.31	0.08 ± 0.03	3.36 ± 1.06	1.64 ± 0.47	0.33 ± 0.18	0.29 ± 0.05	2.31 ± 0.24
S. int.	1.13 ± 0.63	0.04 ± 0.01	0.03 ± 0.01	3.95 ± 0.73	0.24 ± 0.04	0.18 ± 0.07	1.47 ± 0.46	0.18 ± 0.08	0.04 ± 0.01	1.75 ± 0.16	0.66 ± 0.12	0.16 ± 0.07	0.18 ± 0.02	1.29 ± 0.05
L. int.	1.06 ± 0.19	0.04 ± 0.01	0.03 ± 0.01	3.18 ± 0.31	0.28 ± 0.05	0.22 ± 0.07	1.11 ± 0.14	0.15 ± 0.08	0.04 ± 0.01	1.23 ± 0.17	0.44 ± 0.07	0.11 ± 0.04	0.17 ± 0.03	0.95 ± 0.13
Muscle	0.27 ± 0.08	0.01 ± 0.00	0.01 ± 0.00	1.60 ± 0.20	0.08 ± 0.02	0.04 ± 0.01	0.66 ± 0.07	0.11 ± 0.04	0.02 ± 0.00	0.68 ± 0.14	0.40 ± 0.07	0.11 ± 0.03	0.08 ± 0.02	0.64 ± 0.06
Bone	0.46 ± 0.10	0.02 ± 0.01	0.02 ± 0.01	2.18 ± 0.71	0.10 ± 0.02	0.06 ± 0.02	1.11 ± 0.14	0.14 ± 0.03	0.05 ± 0.02	1.63 ± 0.50	0.66 ± 0.14	0.15 ± 0.05	0.09 ± 0.01	0.85 ± 0.19
Skin	1.03 ± 0.28	0.04 ± 0.01	0.03 ± 0.01	5.19 ± 1.10	0.33 ± 0.09	0.19 ± 0.06	2.41 ± 0.21	0.31 ± 0.09	0.05 ± 0.01	2.89 ± 0.52	1.61 ± 0.40	0.44 ± 0.35	0.32 ± 0.04	3.02 ± 0.13
Brain	0.07 ± 0.01	0.00 ± 0.00	0.01 ± 0.00	0.37 ± 0.09	0.02 ± 0.01	0.03 ± 0.01	0.23 ± 0.02	0.02 ± 0.01	0.01 ± 0.00	0.45 ± 0.13	0.15 ± 0.02	0.04 ± 0.01	0.02 ± 0.00	0.28 ± 0.03
[% ID]														
Thyroid	7.2 ± 1.1	4.6 ± 1.2	3.7 ± 1.5	13.6 ± 2.74	13.1 ± 8.0	23.58 ± 6.0	4.2 ± 0.5	3.1 ± 0.3	2.9 ± 1.0	1.5 ± 0.3	3.4 ± 1.7	2.4 ± 0.8	5.0 ± 2.2	2.4 ± 0.5

*Biodistribution was quantified in dual tracer experiments in the combinations ^{125}I-Fab / ^{124}I-Fab-PAS$_{200}$ and ^{125}I-Fab-PAS$_{100}$ / ^{124}I-Fab-PAS$_{400}$.

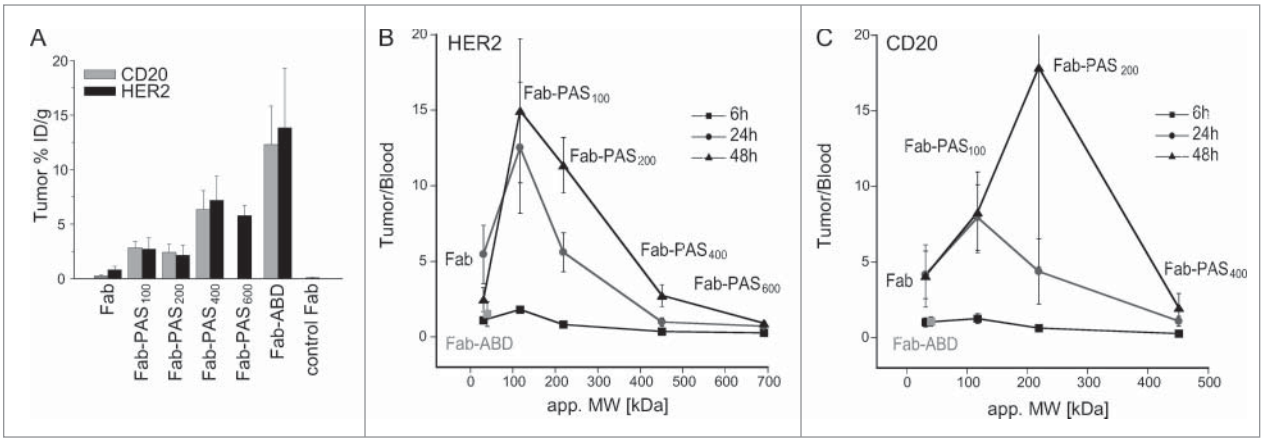

Figure 3. Correlation of tumor uptake and tumor-to-blood ratio with plasma half-life. CD1-*Foxn1*^{nu} mice bearing s.c. SK-BR-3 or Granta xenografts in the right shoulder were injected with ^{125}I-labeled Fabs. (**A**) Tracer uptake for HER2- and CD20-positive tumors 24 h p.i. quantified in a γ-counter for various PASylated Fabs (mean values ± standard deviation; n = 5). The IN-1 Fab served as negative control. (**B, C**) Tumor-to-blood ratio plotted against the apparent molecular size (MW) – correlating both with the length of the attached PAS tag and with plasma half-life[36] – of the different PASylated αHER2 (**B**) and αCD20 (**C**) Fabs 6 h, 24 h and 48 h p.i. (n = 5). Data points for Fab-ABD are shown for comparison in gray.

($p < 0.05$ and $p < 0.001$). Similarly, in analogous control experiments with CD20-positive xenografts, tumor uptake of radio-iodinated αCD20 Fab-PAS$_{200}$ was effectively blocked with a 1,000-fold excess of rituximab (0.68% ID/g *vs.* 2.41% ID/g; 24 h p.i.; $p < 0.05$; cf. **Table 2**). It should be noted that rituximab recognizes loop regions of CD20 in close proximity to the ofatumumab epitope,[38] such that binding of the corresponding Fab is prevented in a competitive manner.

Relationship between tumor-to-blood ratio and pharmacokinetics of PASylated Fabs

The tumor-to-blood ratios determined in the biodistribution studies for the αHER2 and αCD20 Fabs with PAS tags of different lengths described above were plotted against their apparent molecular sizes (**Fig. 3**), which were previously determined by analytical SEC and are known to correlate with plasma half-life in mice.[36] For both αHER2 and αCD20 Fab versions the resulting graphs revealed a bell-shaped curve, both at 24 h and at 48 h p.i., starting at a low level for the unmodified Fabs, followed by an initial increase due to PASylation, with a pronounced optimum occurring in the range of 100 to 200 PAS residues.

In fact, excellent tumor-to-blood and tumor-to-normal tissue ratios, with 12.2 in the case of HER2 and 7.5 in the case of CD20, were observed for Fab-PAS$_{100}$ 24 h p.i. While tumor-to-blood ratios for the αHER2 Fab-PAS$_{200}$ were comparable to the unmodified Fab at this time point, the Fab-PAS$_{200}$ format revealed similar or even better tumor-to-blood ratio than the 100 residue PAS tag at 48 h p.i., especially in the case of the corresponding αCD20 Fab version (cf. **Fig. 3B and 3C**). This behavior was most likely the result of a longer contact and accumulation time due to the slower plasma clearance and possibly also to a reduced wash-out from tumor tissue. Taken together, based on these data both Fab-PAS$_{100}$ and Fab-PAS$_{200}$ constructs appear clearly superior for in vivo imaging purposes in comparison with the unmodified Fabs.

When further increasing the molecular size of the Fabs via fusion with PAS sequences of greater length, i.e., with 400 or 600 residues, the circulation time in blood was extended to a similar level as with the ABD.[36] Interestingly, under these conditions the high blood radioactivity 24 h p.i. led to decreased tumor-to-blood ratios as well as poor imaging contrast, thus approaching the unfavorable imaging properties of full-size antibodies.

Time-dependent biodistribution and PET imaging of αHER2 and αCD20 Fab-PAS$_{200}$

Since the Fab-PAS$_{200}$ format had essentially shown optimal tumor accumulation in the preceding experiments, sequential static PET scans were performed 6 h, 24 h and 120 h p.i. to investigate the distribution of both αHER2 and αCD20 Fab-PAS$_{200}$ over time (**Fig. 4**). The best imaging contrast was seen 24 h p.i. for both tracers, while even after 120 h signals were still detectable in the tumor. Upon antigen blocking with a 1,000-fold excess of trastuzumab or rituximab, representative PET-images 24 h p.i. showed strong reduction in tumor uptake, confirming the previously observed high specificity of these protein tracers. Detailed biodistribution analyses 6 h, 24 h and 48 h p.i. further revealed that already 24 h p.i. both αHER2 and αCD20 Fab-PAS$_{200}$ versions were almost entirely cleared from blood and normal tissue (**Fig. 4C, 4D**), thus resulting in the high tumor contrast.

Discussion

For clinical tumor imaging the use of smaller functional fragments instead of full size mAbs has shown promise, in particular with regard to their faster blood clearance and better tumor penetration.[25,26] While scFvs, which constitute the smallest kind of functional Ig fragments, are somewhat easier to prepare in form of recombinant proteins, they often show an oligomerization

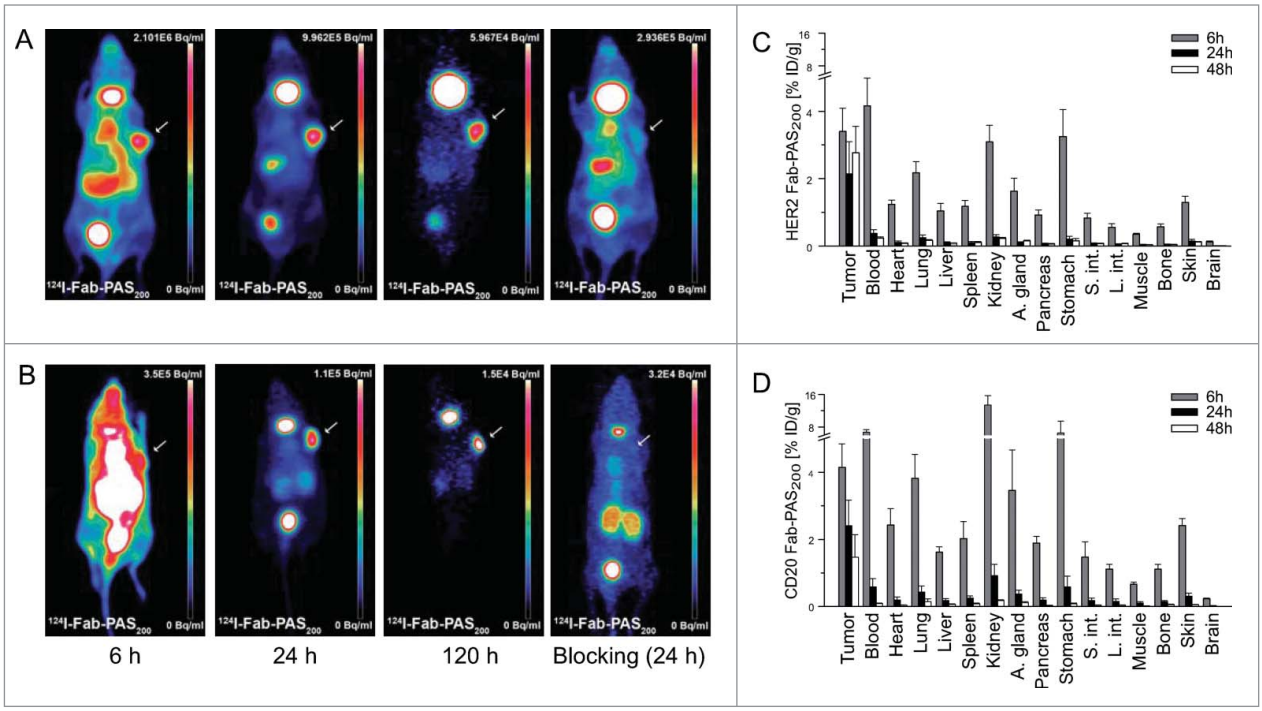

Figure 4. Evaluation of the Fab-PAS$_{200}$ format as radioactive imaging tracer. (**A, B**) PET scans were recorded at varying time points on CD1-*Foxn1*^{nu} mice carrying s.c. HER2-positive (SK-BR-3) or CD20-positive (Granta) tumors (see arrows) after administration of ^{124}I-Fab-PAS$_{200}$. Sequential MIP images were collected 6 h, 24 h, and 120 h p.i. for HER2 (**A**) and CD20 (**B**). To investigate tumor target blocking in a control experiment, 0.56 mg trastuzumab or rituximab, respectively, was injected both 24 h before and together with the radiolabeled Fab, followed by scanning 24 h p.i. as above. For each tumor type, Fab-PAS$_{200}$ shows increasing contrast over time and stable tumor uptake till 120 h after injection. Note that thyroid was not blocked for iodine uptake (as in **Fig. 2**). (**C, D**) Biodistribution analysis of radio-iodinated αHER2 (**C**) and αCD20 (**D**) Fab-PAS$_{200}$, illustrating the percentage of injected dose per gram (% ID/g) 6 h, 24 h and 48 h p.i. (mean values ± standard deviation; n = 5).

tendency, thus resulting in inhomogeneous preparations with variations in molecular size and target avidity. In contrast, Fabs offer clear benefits with regard to much higher protein stability, which also has led to several biopharmaceutical products.[1] In fact, several Fabs have been approved by the FDA or the European Medicines Agency as imaging reagents for single photon emission computed tomography (SPECT): ^{99m}Tc-arcitumomab (CEA-Scan),[54] ^{99m}Tc-sulesomab (LeukoScan)[55] and ^{99m}Tc-bectumomab (LymphoScan).[56]

Compared with full-size mAbs, Fabs have a much shorter plasma half-life (approximately by a factor 30 – in humans)[57] due to their lack of FcRn-mediated recycling and their smaller size, which boosts renal elimination. The shorter circulation is generally considered beneficial for in vivo imaging because it (i) allows better tumor/tissue penetration, and (ii) leads to quick clearance of background radioactivity in the blood. However, the small monovalent Fabs, which cannot take advantage of an avidity effect such as bivalent IgGs, also tend to diffuse out of the tumor when their plasma concentration drops, thus lowering the effective tumor uptake. Consequently, apart from antigen affinity, there is also an interdependent relationship between molecular size and circulation half-life of a protein tracer with regard to tumor targeting efficacy, which was previously noted by others, too.[27,35,58]

Recent analyses of literature data[58,59] from applications of various radiotracers for tumor imaging or cancer therapy indicated how molecular size of the radioconjugate in relation to antigen affinity can influence selective tumor targeting. While the affinity for the cell-surface receptor directly correlates with tumor accumulation, the molecular diameter has mixed effects on several parameters like capillary extravasation from blood, diffusion across the tumor interstitium, available volume fraction in the tumor and, in particular, circulation time. Astonishingly, a theoretical model of tumor targeting[58] predicted lowest tumor uptake for agents of intermediate size with a molecular weight around 25 kDa. Whereas smaller compounds accumulate more rapidly in the tumor, they require higher target affinity in order to achieve similar tumor retention as larger molecules. On the other hand, larger molecules, including mAbs, take advantage of the enhanced permeability and retention effect (EPR). According to these considerations, tumor-targeting properties of mid-size protein tracers may be improved by increasing their molecular dimensions, in line with prolonged plasma half-life.

In this study, we optimized the PK properties of αHER2 and αCD20 Fabs by applying PASylation technology. PASylation offers an ideal tool for such an endeavor as the increase in molecular size, and the resulting retarding effect on kidney filtration, can be smoothly tuned on the genetic level by

varying the length of the encoded PAS polypeptide as part of the recombinant Fab fusion protein.[36] The possibility to directly adjust the parameter plasma half-life of a protein tracer, here Fab, using PAS tags of different lengths without affecting its target-binding activity provides the opportunity to investigate the relation between circulation time, molecular size and tumor-to-blood ratio in an unbiased manner. Remarkably, PET imaging and biodistribution studies of all PASylated Fabs did not show unfavorable accumulation in any normal tissue, thus confirming the biologically inert behavior of the PAS polypeptides and demonstrating that PASylation is compatible with in vivo imaging in general.

As a result, especially the Fab-PAS_{100} and Fab-PAS_{200} formats which carry PAS tags of moderate lengths exhibited excellent tumor-to-blood and tumor-to-normal tissue ratios and, thus, offer promising tracers for clinical applications. Specific binding to HER2 and CD20 tumor antigens was verified by competitive blocking experiments with the cognate antibodies trastuzumab or rituximab. Absence of non-specific tissue staining was confirmed by applying the human NogoA-specific Fab IN1, whose central nervous system antigen is not accessible for circulating antibodies, as a negative control.

Both unmodified αHER2 and αCD20 Fabs showed rapid blood clearance and, consequently, were washed out from tissues and tumor over time, as expected for these small proteins with short plasma half-lives of around 1.3 h in mice, as previously determined for the 4D5 Fab.[36] However, by fusing the recombinant Fabs with PAS sequences of increasing lengths, it was possible to successively prolong their circulation time resulting in increasing tumor accumulation, similar to the effect previously described for PEGylated antibody fragments.[34,60] In our study, maximal tumor uptake 24 h p.i. was seen for Fab-PAS_{400}, which has a plasma half-life of around 14 h in mice and a hydrodynamic volume of 451 kDa as previously determined by analytical SEC.[36] The larger fusion protein Fab-PAS_{600} with its further prolonged circulation time, which was investigated in the case of the αHER2 Fab, showed slightly lower tumor accumulation at this time point, but may not yet have reached its maximum.

Whereas Fab-ABD showed good tumor-to-normal tissue ratios, albumin binding was obviously accompanied by a high level of radioactivity in the blood and, consequently, led to a poor tumor-to-blood ratio, almost like for a full-length mAb. Compared with Fab-PAS_{600}, the similarly extended plasma half-life of 28 h for Fab-ABD with its intrinsically much smaller molecular size (in the absence of albumin) seemed to result in even higher tumor accumulation, in line with a previous study that utilized an albumin-binding peptide fused to the trastuzumab Fab.[27] This may be due to the well-known phenomenon that albumin itself is actively taken up by the tumor, probably as a nutrient supply.[31,32]

Interestingly, in a study using the αHER2 affibody ^{114m}In-CHX-A"-DTPA-ABD-$(Z_{HER2:342})_2$, a similar biodistribution pattern was observed in nude mice bearing LS174T xenografts, revealing 14.5% ID/g in the tumor and 12.6% ID/g in the blood 18 h p.i.[61] Taken together, this indicates that the tumor targeting behavior of albumin-binding agents is only partially dependent on the properties of the antigen-specific module of the protein tracer, at least for HER2-positive xenograft tumors and at earlier time points. In fact, an albumin-mediated tumor accumulation of Fab-ABD might also be responsible for the incomplete blocking with trastuzumab as observed here in the control experiments.

Previous experiments with a PEGylated αHER2 scFv (4D5-PEG20) in an SK-OV-3 tumor xenograft model[35] showed that tumor accumulation can also be boosted by extending the plasma half-life using an albumin-independent biophysical principle. However, this resulted in a much lower tumor-to-blood ratio 24 h p.i. compared to the unmodified protein tracer. These findings are in agreement with our observations for those Fab constructs having a circulation time $\geq$14 h, i.e., Fab-PAS_{400} and Fab-PAS_{600}.

Conversely, much improved tumor-to-blood ratios were observed for Fab-PAS_{100} (24 h p.i.) and Fab-PAS_{200} (48 h p.i.) compared to the unmodified αHER2 and αCD20 Fabs. Thus, it seems that a plasma half-life in mice of 2.7 h or 5.2 h, respectively, and an effective molecular size of 117 kDa or 219 kDa for Fab-PAS_{100} and Fab-PAS_{200}[36] provide a favorable combination between tracer size and circulation time for tumor targeting in a diagnostic setting. In fact, the higher apparent molecular weight and the moderately prolonged circulation led to a 3-fold (HER2) and 12-fold (CD20) increased tumor uptake compared to the unmodified Fabs. Furthermore, a 2-fold improved tumor-to-blood ratio for Fab-PAS_{100} 24 h p.i. and a 2-4-fold improvement for Fab-PAS_{200} 48 h p.i. were observed in the biodistribution analyses for HER2- and CD20-positive tumors.

Interestingly, the hydrodynamic volume of the larger fusion proteins is actually in the range of full-size IgGs, but does not seem to hinder efficient tumor accumulation. In this regard, it has to be kept in mind that PASylated proteins do not quite behave like solid globular proteins (such as albumin or an antibody), rather the dynamically disordered random coil nature of the slim, linear PAS polypeptide confers enhanced diffusional properties in a crowded molecular environment, similar to PEG.[36] Consequently, at least for the PAS fusions with moderate lengths, the effect of prolonged plasma half-life and, hence, extended tumor contact time, which allows enduring tumor accumulation, comes fully into play. Indeed, αHER2 Fab-PAS_{200} showed ongoing tumor uptake between 24 h and 48 h p.i., which probably results from maintaining a concentration gradient between blood plasma and tumor over a longer period of time, as previously discussed by others.[27,35] Therefore, both the Fab-PAS_{100} and the Fab-PAS_{200} format should be suitable candidates for clinical application, depending on the optimal time point for read out, offering enhanced tumor-to-normal tissue ratios and also improved tumor uptake.

Our findings are in agreement with several previous studies on radiolabelled mAbs or antibody fragments that target the tumor antigen HER2. For example, biodistribution of ^{111}In-DOTA-trastuzumab and ^{111}In-DOTA-F(ab')$_2$-trastuzumab showed specific tumor uptake (31 and 20% ID/g, respectively, 24 h p.i.) in mice bearing HER2 positive BT-474 tumor xenografts.[62] In spite of the generally higher tumor accumulation, which might be due

to the larger size of these protein tracers and the use of a residualizing radiometal ion, better tumor-to-blood ratios of 5.3 for the unmodified Fab and even of 12.2 for Fab-PAS_{100} were reached in our study, compared to 3.4 for trastuzumab and 10 for the corresponding $F(ab')_2$.

The CD20-targeting mAb $^{99m}Tc/^{188}Re(CO)_3$-RTXred (rituximab) showed rather low tumor uptake of 0.8-2.7% ID/g at 24 h p.i. in mice bearing a Ramos lymphoma xenograft, depending on the radioisotope, and a poor tumor-to-blood ratio of 0.5. In contrast, an engineered dimeric scFv fusion protein derived from rituximab, the ^{124}I-minibody, revealed clearly higher tumor uptake (13% ID/g) and tumor-to-blood ratio (4.8) 21 h p.i. using the murine B-cell lymphoma cell line 38C13 transduced with human CD20 in a xenograft model.[63,64] For comparison, the monomeric αCD20 Fab-PAS_{100} and Fab-PAS_{200} constructs analyzed in our study showed somewhat lower total tumor accumulation of 2.8 and 2.4% ID/g 24 h p.i., but also considerably lower blood and normal tissue burden, thus yielding better imaging contrast 24 h p.i., with tumor-to-blood ratios of 4-8.

In a previous study on the role of PK for tumor targeting, two versions of a $^{99m}Tc(CO)_3$-labeled scFv derived from trastuzumab were investigated: the small monomeric antibody fragment itself and the corresponding scFv chemically conjugated to 20 kDa linear PEG.[35] Although PEGylation led to a marked decrease in antigen affinity in this study, contrasting with PASylation, these two molecules appear comparable to the αHER2 Fab and Fab-PAS_{400} constructs, respectively, with regard to plasma half-life.[36] PEGylation of the αHER2 scFv led to a 5-fold increase in tumor accumulation from 1.7% ID/g (monomer) to 9.3% ID/g (monomer-PEG20k) at 24 h p.i. while PASylation with 400 residues of the αHER2 Fab resulted in a 9-fold (for HER2) to 26-fold (for CD20) increase in tumor uptake in our study. Interestingly, in both cases the tumor-to-blood ratio was concomitantly decreased, 4-fold for the scFv coupled to PEG20k and 4-5-fold for the Fab fused to 400 PAS residues.

A similar effect of molecular size increase by PEGylation was observed for HER2-specific DARPins, an engineered non-Ig protein scaffold, in a SK-OV-3 mouse xenograft model.[34] In this report, conjugation to PEG20k led to a 1.6-5-fold improved tumor uptake, depending on the affinity of the investigated DARPin, but also to lower tumor-to-blood ratio. Thus, if compared according to molecular size, both PASylation and PEGylation show similar effects on tumor uptake of the tracers used for in vivo imaging, which is in agreement with the analogous biophysical properties of both polymers and their prolonging effect on circulation.[36]

Nevertheless, a more modest extension of plasma half-life in the range of 2-14 h has not been described up to now. In fact, our study demonstrates for the first time that prolongation of circulation just by a factor 2-3 compared with the unmodified recombinant Fab considerably improves tumor-to-blood ratio, as was observed here for Fab-PAS_{100} (24 h p.i.) and Fab-PAS_{200} (48 h p.i.). Apparently, such positive effects on imaging contrast were missed by the previous PEGylation studies, since only rather large PEG polymers (20, 40 or 60 kDa) were investigated.[34,35] Instead, PAS polypeptides with 100-200 residues would correspond to 5-10 kDa PEG chains with regard to molecular size as well as retardation of kidney clearance. Consequently, for effective tumor targeting of the protein tracer and, in particular, high imaging contrast, a moderate increase in the hydrodynamic molecular volume is crucial to achieve an optimum between plasma concentration / circulation time and tissue penetration / tumor accumulation.

Apart from that, compared to chemical conjugation with PEG, which is a synthetic polymer with inherent size polydispersity, PASylation yields a truly uniform protein preparation, avoids laborious in vitro coupling procedures, and does not interfere with the biological activity or affinity of the protein, as was specifically demonstrated for the αHER2 Fab before.[36] This offers a convenient route to quickly generate superior Fab reagents from cloned humanized antibodies to also address other disease-relevant antigens for in vivo imaging applications, taking advantage of an already clinically-approved class of tracer molecules. Furthermore, it even seems that PASylation may improve the in vivo stability of the radiolabeled Fab fragments since Fab-PAS_{200}, Fab-PAS_{400} and Fab-PAS_{600} showed less accumulation of free iodide in the thyroid, otherwise an indication for proteolysis, dehalogenation and metabolization.[65] Finally, PASylation also appeared to prevent overt accumulation in the kidneys.

Neglecting effects of allometric scaling when transferring preclinical data from mice to man, the two PASylated αHER2 Fab versions with superior tumor imaging properties, Fab-PAS_{100} and Fab-PAS_{200}, may also offer promising tracer reagents for in vivo imaging of pathological HER2 expression in patients. Thus, they could be useful for the diagnosis of HER2-positive tumor recurrence, dose optimization for HER2-targeted therapy and for monitoring of tumor treatment efficiency in a clinical setting. Likewise, the αCD20 Fab-PAS_{200} version appears attractive for noninvasive in vivo monitoring of B-cell lymphoma growth and metastasis, both in animal models during preclinical research and in human therapy.

In conclusion, a few attempts to specifically tailor the plasma half-life of radiolabelled monovalent antibody fragments (Fab or scFv) for imaging and/or tumor targeting have been reported before, which made use of (i) PEGylation[35] and (ii) albumin association.[27] In both cases, significantly higher tumor accumulation in comparison with the unmodified antibody fragment was described. However, this effect, which should be beneficial for radiotherapy, came at the expense of a diminished tumor-to-blood ratio, a parameter crucial for in vivo imaging, obviously because of the much longer persistence of the modified proteins in circulation. Hence, there are two major opposing effects of PK extension: longer perfusion of the tumor leads to higher accumulation of the tracer – owing to the slow dissociation rate once the antibody fragment has bound to its antigen, which is often followed by receptor endocytosis – while at the same time there is a stronger background of radioactivity in the blood and an associated exposure of highly vascularized organs.

In these previous investigations, the tumor-to-blood ratio was eventually improved by performing imaging or biodistribution analyses at later time points, i.e., 48 h p.i. and beyond. In the present study, we followed a different approach: taking advantage

of the easily applicable PASylation technology that offers a purely biophysical and biologically inert way to retard kidney filtration, the plasma half-life was systematically varied about a wide range employing the same Fab fragment as targeting module, thereby avoiding influences on affinity, valency or albumin/FcRn-binding effects upon changing molecular formats. Thus, we found that there is an optimum for plasma half-life / molecular size, which lies around 100-200 PAS residues, roughly equivalent to a single PEG chain of 5-10 kDa. Notably, the same trend was observed for two different Fabs, targeting HER2 and CD20, respectively, which also differed in their antigen affinities by a factor 3.6. This clearly indicates a general mechanism and strongly suggests that PK should be worth optimizing for biomolecular imaging reagents. Beyond that, the beneficial effect of PASylation on specific tumor accumulation demonstrated here should also be applicable to drug conjugates of antibody fragments (or alternative binding proteins) in a therapeutic setting.

Materials and Methods

Preparation of recombinant αHER2 and αCD20 Fabs

The following amino acid exchanges were introduced via QuikChange mutagenesis (Stratagene, La Jolla, CA) into a version of the trastuzumab Fab that was previously cloned on the bacterial expression vector pASK88:[40] $K^{H3}Q$, $Q^{H5}V$, $E^{L3}Q$, $L^{L4}M$ and $L^{L104}V$. In addition, the amino acid substitution $D^{H98}W$ (Kabat numbering) was introduced to improve the affinity for the HER2 tumor antigen.[41] Also, the mutated V-genes were subcloned via *Xba*I and *Sac*II on the vector pASK106-4D5[66] to produce the Fab as fusion protein with the ABD from *Streptococcal* protein G at the C-terminus of its light chain.[40] Corresponding Fabs fused with PAS polypeptides of different lengths were prepared using a recently published series of compatible expression plasmids.[36]

The V-genes corresponding to the amino acid sequence of ofatumumab[14] were obtained by gene synthesis (Mr. Gene, Regensburg, Germany) and subcloned via standardized restriction sites on pASK88, providing human $C_H1\gamma_1$ and Cκ constant domain regions, to yield the αCD20 Fab.[42] After that, appropriate derivative plasmids were constructed by subcloning as above to express analogous fusion proteins as for the αHER2 Fab.

The different Fab versions were produced in *E. coli* JM83 at 22°C in shake flasks using LB medium containing 100 mg/l ampicillin according to a published procedure.[40] In case of the PASylated Fabs, 6 g/l glucose and 1 g/l proline were added. Three hours after induction at $OD_{550} = 0.5$ with 200 μg/l anhydrotetracycline (Acros Organics, Geel, Belgium) bacterial cells were harvested by centrifugation and the periplasmic extract was prepared.[67] The dialyzed protein fraction was applied to a Zn(II)-charged IDA Sepharose column and eluted with an imidazole/HCl concentration gradient.[67, 68] Fabs fused to PAS_{400} and PAS_{600} sequences were further purified via *Strep*-Tactin affinity chromatography utilizing the *Strep*-tag II[69] at the C-terminus of the PAS tag that was appended to the light chain. To isolate monodisperse protein and deplete bacterial endotoxin, SEC on a Superdex 200 HR 10/300 GL column (GE Healthcare, Munich, Germany), as well as ion exchange chromatography on Q-Sepharose (GE Healthcare), were performed using phosphate-buffered saline (PBS; 4 mM KH_2PO_4, 16 mM Na_2HPO_4, 115 mM NaCl) as running buffer.

The purified recombinant Fabs were concentrated by ultrafiltration (Amicon Ultra centrifugal filter devices 30,000 MWCO; Millipore, Billerica, MA). Purity and disulfide bond formation was analyzed by SDS-PAGE and analytical SEC. Protein concentration was determined according to absorption at 280 nm using calculated extinction coefficients[70] of 77405 $M^{-1}cm^{-1}$ for αHER2 Fab and its PASylated versions, 81875 $M^{-1}cm^{-1}$ for αHER2 Fab-ABD, 75915 $M^{-1}cm^{-1}$ for αCD20 Fab and its PASylated versions and 80385 $M^{-1}cm^{-1}$ for αCD20 Fab-ABD.

In vitro binding studies of αHER2 and αCD20 Fabs

The HER2-positive human breast adenocarcinoma cell line SK-BR-3[45] was cultured to 80–90% confluence in Dulbecco's Modified Eagle Medium (DMEM) (Biochrom, Berlin, Germany) supplemented with 10% v/v Fetal Bovine Serum (FBS) (Biochrom) and 1% w/v penicillin/streptomycin at 37°C in a humidified 5% CO_2 atmosphere. Cells were detached with Accutase (Sigma-Aldrich, St. Louis, MO), counted with a Neubauer counting chamber and washed with 10% v/v FBS, 2 mM EDTA, 0.002% w/v sodium azide (FACS buffer). The CD20-positive human mantle cell lymphoma line Granta-519[46] was cultured in DMEM supplemented with 20% v/v FBS.

In each case, 10^5 cells were incubated with 100 μl of the Fab preparation (0.031-512 nM), diluted in FACS buffer, for 1 h at 4°C in a 96-well microtiter plate. After two washing steps with FACS buffer, the cells were incubated with 50 μl of a fluorescein-conjugated αhu-kappa-light chain antibody (Invitrogen / Life Technologies, Darmstadt, Germany) for 20 min at 4°C. Cells were finally centrifuged and resuspended in 500 μl FACS buffer. Then, propidium iodide was added to a final concentration of 1 μg/ml to label (and exclude during counting) dead cells, and antibody-stained cells were counted with a FACSAria Cell-Sorting system (BD Biosciences, Heidelberg, Germany). Data were analyzed using FlowJo software (Tree Star, Ashland, OR) and the mean fluorescence intensity (MFI; normalized against the isotype control) was plotted against the applied concentration of the Fab. The apparent K_D value was fitted using the formula $MFI = \Delta MFI_{max} \cdot [Fab] / (K_D + [Fab])$ and plotted using Kaleidagraph Software (Synergy, Reading, PA) with ΔMFI_{max} set to 100%.

Radio-iodination of Fabs

The purified Fab versions were labeled with various radioactive isotopes of iodine using the Iodogen method,[49] aiming at a molar ratio between iodine and Fab of 1:1 (as specifically adjusted for ^{125}I). Typically, 50 μg Iodogen (Pierce, Rockford, IL) was coated at the bottom of a plastic vial by drying a 1 mg/ml solution in dichloromethane with a gentle argon stream and stored at −20°C. For radiolabeling, 0.44 nmol purified Fab or mAb diluted in 200 μl PBS (1.4 mM KH_2PO_4, 10 mM Na_2HPO_4, 137 mM NaCl, 2.6 mM KCl) was mixed with

37 MBq of either $Na^{125}I$ with a specific activity of 74 MBq/nmol (Hartman Analytic, Braunschweig, Germany), $Na^{123}I$ with a specific activity of 185 MBq/nmol (GE Healthcare, Buckinghamshire, UK), $Na^{124}I$ with a specific activity of ~1.1 MBq/pmol (IBA Molecular, VU Amsterdam, The Netherlands) or 0.5 nmol sodium salt of the stable isotope ^{127}I, each dissolved in 100 µl 1 mM NaOH, and added to the vial. After 15 min incubation at room temperature, the reaction was stopped by addition of 10 µl 25 mg/ml Na-ascorbate/HCl pH 4–5 and the mixture was immediately pipetted out of the plastic vial and, hence, separated from the insoluble oxidizing agent.

Coupling yields of 80-90%, depending on the iodine isotope, were achieved as determined by thin layer chromatography (TLC) on glass micro fiber paper (Agilent Technologies, Santa Clara, CA) using 0.9% w/v NaCl as mobile phase, leading to retention factors (Rf) of 0.0 and 1.0 for the radiolabeled Fab and free iodide, respectively. The radio-iodinated Fabs were separated from excess reagents by gel filtration on a PD-10 column (GE Healthcare) using 5.2 mM histidine/HCl pH 6, 2% w/v trehalose, 0.9% w/v NaCl, 0.009% v/v Tween20 as running buffer, thus preventing loss by adsorption. Radiochemical purity, analyzed by TLC, was >98% for the initial 1 ml elution fraction. A specific activity of approximately 80 MBq/nmol was calculated from the radioactivities of the reagents and the reaction yields. Protein concentration was verified with a micro-Bradford assay (Bio-Rad Protein Assay Kit II; Bio-Rad Laboratories, Hercules, CA). Iodinated Fabs were further analyzed by SDS-PAGE and the ^{127}I-labeled HER2 Fab was tested for in vitro antigen binding activity via FACS titration of tumor cells as described above.

In vivo studies

For biodistribution analyses and PET imaging, female CD1-*Foxn1^{nu}* mice of age 6–8 weeks (Charles River Laboratories, Sulzfeld, Germany) were injected subcutaneously with 5×10^6 SK-BR-3 cells suspended in 100 µl DMEM into the right shoulder. After approximately two weeks, tumors had reached a size of 300-500 mm^3. Alternatively, 5×10^6 Granta-519 cells were mixed with Matrigel Basement Membrane Matrix (BD Biosciences) for subcutaneous injection to achieve more uniform tumor growth over 4–5 weeks, eventually achieving sizes of 300–500 mm^3.

Micro-PET studies were performed after tail-vein injection of 6–12 MBq ^{124}I-labeled Fab having a specific activity of 80 MBq/nmol (n = 2). 60-min static PET images were acquired 6 h, 24 h and 120 h post injection (p.i.) under isoflurane anesthesia on an Inveon PET/CT small animal scanner (Siemens Medical Solutions, Knoxville, TN). Images were reconstructed using a 3-dimensional ordered-subsets expectation maximum algorithm (3D-OSEM) and analyzed using Inveon Research Workplace software (Siemens Medical Solutions). All images are shown as maximum intensity projections (MIP) after scaling to achieve a similar intensity of each tumor, thus allowing better comparison of tumor-to-background ratios.

For biodistribution studies, mice were injected intravenously with 0.37–0.74 MBq of ^{123}I-Fab, ^{124}I-Fab or ^{125}I-Fab (specific activity 80 MBq/nmol). At 6 h, 24 h and 48 h p.i., mice (n = 5–6) were sacrificed in a CO_2 atmosphere, the stomach was emptied, blood and organs of interest were dissected, weighed and analyzed in a Wallac Wizard γ-counter (PerkinElmer, Turku, Finland). The total applied radioactivity was determined by measuring the syringes before and after injection with a CRC-15R Dose Calibrator (Capintec, Ramsey NJ). The percentage of injected dose (% ID), corrected for the dose remaining in the tail, per gram of each organ (% ID/g) was calculated using a standard containing 1% of the injected activity diluted in water.

$^{125}I/^{124}I$ or $^{125}I/^{123}I$ dual tracer experiments for different PASylated Fab combinations directed against the same tumor target were performed as indicated in **Tables 1** and **2**. The different iodine activities were individually quantified in the γ-counter with appropriate calibration. In case of the combination with ^{124}I, which emits high energy γ-radiation, ^{125}I was measured after decay for 10 half-life periods of the former.

For antigen blocking experiments (n = 3–4), 0.56 mg trastuzumab or rituximab from the hospital pharmacy or 0.2 mg Fab-ABD was injected into the tail vein once 24 h before and once together with the radiolabeled Fab.

All animal experiments were approved by local authorities (Regierung von Oberbayern, Germany; license no. 55.2–1–54–2532–46–12) and were in compliance with the local regulatory and institutional guidelines.

Disclosure of Potential Conflicts of Interest

AS and MS are cofounders of XL-protein GmbH, Germany.

Acknowledgments

The authors wish to thank Sabine Pirsig, Katharina McGuire and Andrea Alke for experimental support and Sybille Reder, Markus Mittelhäuser and Marco Lehmann for performing the imaging studies. We are grateful to Prof. Dr. Andreas K. Buck for support in the animal experiments and for providing the Granta cell line and to Prof. Dr. Sibylle Ziegler for discussions regarding PET data analysis.

Funding

This work was supported by the Deutsche Forschungsgemeinschaft (SFB-824) and the European Union Seventh Framework Program (FP7) under Grant Agreement No. 294582 ERC Grant MUMI.

Supplemental Material

Supplemental data for this article can be accessed on the publisher's website.

References

1. Nelson AL, Reichert JM. Development trends for therapeutic antibody fragments. Nat Biotechnol 2009; 27:331-337; PMID:19352366; http://dx.doi.org/10.1038/nbt0409-331
2. Reichert JM. Marketed therapeutic antibodies compendium. MAbs 2012; 4:413-415; PMID:22531442; http://dx.doi.org/10.4161/mabs.19931
3. Dimitrov DS, Marks JD. Therapeutic antibodies: current state and future trends—is a paradigm change coming soon? Methods Mol Biol 2009; 525:1-27; PMID:19252861; http://dx.doi.org/10.1007/978-1-59745-554-1_1
4. Witzig TE, Gordon LI, Cabanillas F, Czuczman MS, Emmanouilides C, Joyce R, Pohlman BL, Bartlett NL, Wiseman GA, Padre N, et al. Randomized controlled trial of yttrium-90-labeled ibritumomab tiuxetan radioimmunotherapy versus rituximab immunotherapy for patients with relapsed or refractory low-grade, follicular, or transformed B-cell non-Hodgkin's lymphoma. J Clin Oncol 2002; 20:2453-2463; PMID:12011122; http://dx.doi.org/10.1200/JCO.2002.11.076
5. Slamon DJ, Clark GM, Wong SG, Levin WJ, Ullrich A, McGuire WL. Human breast cancer: correlation of relapse and survival with amplification of the HER-2/neu oncogene. Science 1987; 235:177-182; PMID:3798106; http://dx.doi.org/10.1126/science.3798106
6. Scholl S, Beuzeboc P, Pouillart P. Targeting HER2 in other tumor types. Ann Oncol 2001; 12 Suppl 1:S81-S87; PMID:11521727; http://dx.doi.org/10.1093/annonc/12.suppl_1.S81
7. Carter P, Presta L, Gorman CM, Ridgway JB, Henner D, Wong WL, Rowland AM, Kotts C, Carver ME, Shepard HM. Humanization of an anti-p185^{HER2} antibody for human cancer therapy. Proc Natl Acad Sci U S A 1992; 89:4285-4289; PMID:1350088; http://dx.doi.org/10.1073/pnas.89.10.4285
8. Baselga J. Clinical trials of Herceptin (trastuzumab). Eur J Cancer 2001; 37 Suppl 1:S18-S24; PMID:11167087; http://dx.doi.org/10.1016/S0959-8049(00)00404-4
9. Dirix LY, Rutten A, Huget P, Dirix M. Trastuzumab emtansine in breast cancer. Expert Opin Biol Ther 2013; 13:607-614; PMID:23477731; http://dx.doi.org/10.1517/14712598.2013.778238
10. Eisenberg R, Looney RJ. The therapeutic potential of anti-CD20: "What do B-cells do?". Clin Immunol 2005; 117:207-213; PMID:16169773; http://dx.doi.org/10.1016/j.clim.2005.08.006
11. Kosmas C, Stamatopoulos K, Stavroyianni N, Tsavaris N, Papadaki T. Anti-CD20-based therapy of B cell lymphoma: state of the art. Leukemia 2002; 16:2004-2015; PMID:12357351; http://dx.doi.org/10.1038/sj.leu.2402639
12. Lemery SJ, Zhang J, Rothmann MD, Yang J, Earp J, Zhao H, McDougal A, Pilaro A, Chiang R, Gootenberg JE, et al. U.S. Food and Drug Administration approval: ofatumumab for the treatment of patients with chronic lymphocytic leukemia refractory to fludarabine and alemtuzumab. Clin Cancer Res 2010; 16:4331-4338; PMID:20601446; http://dx.doi.org/10.1158/1078-0432.CCR-10-0570
13. Hagenbeek A, Gadeberg O, Johnson P, Pedersen LM, Walewski J, Hellmann A, Link BK, Robak T, Wojtukiewicz M, Pfreundschuh M, et al. First clinical use of ofatumumab, a novel fully human anti-CD20 monoclonal antibody in relapsed or refractory follicular lymphoma: results of a phase 1/2 trial. Blood 2008; 111:5486-5495; PMID:18390837; http://dx.doi.org/10.1182/blood-2007-10-117671
14. Teeling JL, French RR, Cragg MS, van den Brakel J, Pluyter M, Huang H, Chan C, Parren PW, Hack CE, Dechant M, et al. Characterization of new human CD20 monoclonal antibodies with potent cytolytic activity against non-Hodgkin lymphomas. Blood 2004; 104:1793-1800; PMID:15172969; http://dx.doi.org/10.1182/blood-2004-01-0039
15. Milenic DE, Brady ED, Brechbiel MW. Antibody-targeted radiation cancer therapy. Nat Rev Drug Discov 2004; 3:488-499; PMID:15173838; http://dx.doi.org/10.1038/nrd1413
16. van Dongen GA, Poot AJ, Vugts DJ. PET imaging with radiolabeled antibodies and tyrosine kinase inhibitors: immuno-PET and TKI-PET. Tumour Biol 2012; 33:607-615; PMID:22270450; http://dx.doi.org/10.1007/s13277-012-0316-4
17. Dijkers EC, Oude Munnink TH, Kosterink JG, Brouwers AH, Jager PL, de Jong JR, van Dongen GA, Schroder CP, Lub-de Hooge MN, de Vries EG. Biodistribution of ^{89}Zr-trastuzumab and PET imaging of HER2-positive lesions in patients with metastatic breast cancer. Clin Pharmacol Ther 2010; 87:586-592; PMID:20357763; http://dx.doi.org/10.1038/clpt.2010.12
18. Gaykema SB, Brouwers AH, Hovenga S, Lub-de Hooge MN, de Vries EG, Schroder CP. Zirconium-89-trastuzumab positron emission tomography as a tool to solve a clinical dilemma in a patient with breast cancer. J Clin Oncol 2012; 30:e74-75; PMID:22203768; http://dx.doi.org/10.1200/JCO.2011.38.0204
19. Divgi CR, Pandit-Taskar N, Jungbluth AA, Reuter VE, Gonen M, Ruan S, Pierre C, Nagel A, Pryma DA, Humm J, et al. Preoperative characterisation of clear-cell renal carcinoma using iodine-124-labelled antibody chimeric G250 (124I-cG250) and PET in patients with renal masses: a phase I trial. Lancet Oncol 2007; 8:304-310; PMID:17395103; http://dx.doi.org/10.1016/S1470-2045(07)70044-X
20. Lobo ED, Hansen RJ, Balthasar JP. Antibody pharmacokinetics and pharmacodynamics. J Pharm Sci 2004; 93:2645-2668; PMID:15389672; http://dx.doi.org/10.1002/jps.20178
21. Iyer AK, Khaled G, Fang J, Maeda H. Exploiting the enhanced permeability and retention effect for tumor targeting. Drug Discov Today 2006; 11:812-818; PMID:16935749; http://dx.doi.org/10.1016/j.drudis.2006.07.005
22. Wester HJ, Kessler H. Molecular targeting with peptides or peptide-polymer conjugates: just a question of size? J Nucl Med 2005; 46:1940-1945; PMID:16330555
23. Dreher MR, Liu W, Michelich CR, Dewhirst MW, Yuan F, Chilkoti A. Tumor vascular permeability, accumulation, and penetration of macromolecular drug carriers. J Natl Cancer Inst 2006; 98:335-344; PMID:16507830; http://dx.doi.org/10.1093/jnci/djj070
24. Wu AM, Senter PD. Arming antibodies: prospects and challenges for immunoconjugates. Nat Biotechnol 2005; 23:1137-1146; PMID:16151407; http://dx.doi.org/10.1038/nbt1141
25. Holliger P, Hudson PJ. Engineered antibody fragments and the rise of single domains. Nat Biotechnol 2005; 23:1126-1136; PMID:16151406; http://dx.doi.org/10.1038/nbt1142
26. Kenanova V, Wu AM. Tailoring antibodies for radionuclide delivery. Expert Opin Drug Deliv 2006; 3:53-70; PMID:16370940; http://dx.doi.org/10.1517/17425247.3.1.53
27. Dennis MS, Jin H, Dugger D, Yang R, McFarland L, Ogasawara A, Williams S, Cole MJ, Ross S, Schwall R. Imaging tumors with an albumin-binding Fab, a novel tumor-targeting agent. Cancer Res 2007; 67:254-261; PMID:17210705; http://dx.doi.org/10.1158/0008-5472.CAN-06-2531
28. Thurber GM, Zajic SC, Wittrup KD. Theoretic criteria for antibody penetration into solid tumors and micrometastases. J Nucl Med 2007; 48:995-999; PMID:17504872; http://dx.doi.org/10.2967/jnumed.106.037069
29. Baker K, Qiao SW, Kuo T, Kobayashi K, Yoshida M, Lencer WI, Blumberg RS. Immune and non-immune functions of the (not so) neonatal Fc receptor, FcRn. Semin Immunopathol 2009; 31:223-236; PMID:19495758; http://dx.doi.org/10.1007/s00281-009-0160-9
30. Chaudhury C, Mehnaz S, Robinson JM, Hayton WL, Pearl DK, Roopenian DC, Anderson CL. The major histocompatibility complex-related Fc receptor for IgG (FcRn) binds albumin and prolongs its lifespan. J Exp Med 2003; 197:315-322; PMID:12566415; http://dx.doi.org/10.1084/jem.20021829
31. Stehle G, Sinn H, Wunder A, Schrenk HH, Stewart JC, Hartung G, Maier-Borst W, Heene DL. Plasma protein (albumin) catabolism by the tumor itself – implications for tumor metabolism and the genesis of cachexia. Crit Rev Oncol Hematol 1997; 26:77-100; PMID:9298326; http://dx.doi.org/10.1016/S1040-8428(97)00015-2
32. Merlot AM, Kalinowski DS, Richardson DR. Unraveling the mysteries of serum albumin—more than just a serum protein. Front Physiol 2014; 5:299; PMID:25161624; http://dx.doi.org/10.3389/fphys.2014.00299
33. Pasut G, Veronese FM. State of the art in PEGylation: the great versatility achieved after forty years of research. J Control Release 2012; 161:461-472; PMID:22094104; http://dx.doi.org/10.1016/j.jconrel.2011.10.037
34. Zahnd C, Kawe M, Stumpp MT, de Pasquale C, Tamaskovic R, Nagy-Davidescu G, Dreier B, Schibli R, Binz HK, Waibel R, et al. Efficient tumor targeting with high-affinity designed ankyrin repeat proteins: effects of affinity and molecular size. Cancer Res 2010; 70:1595-1605; PMID:20124480; http://dx.doi.org/10.1158/0008-5472.CAN-09-2724
35. Kubetzko S, Balic E, Waibel R, Zangemeister-Wittke U, Plückthun A. PEGylation and multimerization of the anti-p185^{HER-2} single chain Fv fragment 4D5. Effects on tumor targeting. J Biol Chem 2006; 281:35186-35201; PMID:16963450; http://dx.doi.org/10.1074/jbc.M604127200
36. Schlapschy M, Binder U, Börger C, Theobald I, Wachinger K, Kisling S, Haller D, Skerra A. PASylation: a biological alternative to PEGylation for extending the plasma half-life of pharmaceutically active proteins. Protein Eng Des Sel 2013; 26:489-501; PMID:23754528; http://dx.doi.org/10.1093/protein/gzt023
37. Binder U, Skerra A. Half-life extension of therapeutic proteins via genetic fusion to recombinant PEG mimetics. In: Kontermann R, ed. Therapeutic Proteins – Strategies to Modulate Their Plasma Half-lives. Weinheim, Germany: Wiley-VCH, 2012:63-80.
38. Du J, Yang H, Guo Y, Ding J. Structure of the Fab fragment of therapeutic antibody Ofatumumab provides insights into the recognition mechanism with CD20. Mol Immunol 2009; 46:2419-2423; PMID:19427037; http://dx.doi.org/10.1016/j.molimm.2009.04.009
39. McKeage K, Perry CM. Trastuzumab: a review of its use in the treatment of metastatic breast cancer overexpressing HER2. Drugs 2002; 62:209-243; PMID:11790161; http://dx.doi.org/10.2165/00003495-200262010-00008
40. Schlapschy M, Theobald I, Mack H, Schottelius M, Wester HJ, Skerra A. Fusion of a recombinant antibody fragment with a homo-amino-acid polymer: effects on biophysical properties and prolonged plasma half-life. Protein Eng Des Sel 2007; 20:273-284; PMID:17595342; http://dx.doi.org/10.1093/protein/gzm020
41. Gerstner RB, Carter P, Lowman HB. Sequence plasticity in the antigen-binding site of a therapeutic anti-HER2 antibody. J Mol Biol 2002; 321:851-862; PMID:12206766; http://dx.doi.org/10.1016/S0022-2836(02)00677-0
42. Schiweck W, Skerra A. Fermenter production of an artificial Fab fragment, rationally designed for the antigen cystatin, and its optimized crystallization through constant domain shuffling. Proteins 1995; 23:561-565; PMID:8749852; http://dx.doi.org/10.1002/prot.340230411
43. Kraulis PJ, Jonasson P, Nygren PÅ, Uhlén M, Jendeberg L, Nilsson B, Kördel J. The serum albumin-

binding domain of streptococcal protein G is a three-helical bundle: a heteronuclear NMR study. FEBS Lett 1996; 378:190-194; PMID:8549831; http://dx.doi.org/10.1016/0014-5793(95)01452-7
44. Bandtlow C, Schiweck W, Tai HH, Schwab ME, Skerra A. The *Escherichia coli*-derived F_{ab} fragment of the IgM/κ antibody IN-1 recognizes and neutralizes myelin-associated inhibitors of neurite growth. Eur J Biochem 1996; 241:468-475; PMID:8917444; http://dx.doi.org/10.1111/j.1432-1033.1996.00468.x
45. Holmes WE, Sliwkowski MX, Akita RW, Henzel WJ, Lee J, Park JW, Yansura D, Abadi N, Raab H, Lewis GD, et al. Identification of heregulin, a specific activator of $p185^{erbB2}$. Science 1992; 256:1205-1210; PMID:1350381; http://dx.doi.org/10.1126/science.256.5060.1205
46. Rudolph C, Steinemann D, Von Neuhoff N, Gadzicki D, Ripperger T, Drexler HG, Mrasek K, Liehr T, Claussen U, Emura M, et al. Molecular cytogenetic characterization of the mantle cell lymphoma cell line GRANTA-519. Cancer Genet Cytogenet 2004; 153:144-150; PMID:15350304; http://dx.doi.org/10.1016/j.cancergencyto.2004.01.006
47. De Lorenzo C, Tedesco A, Terrazzano G, Cozzolino R, Laccetti P, Piccoli R, D'Alessio G. A human, compact, fully functional anti-ErbB2 antibody as a novel antitumour agent. Br J Cancer 2004; 91:1200-1204; PMID:15305184
48. Uchiyama S, Suzuki Y, Otake K, Yokoyama M, Ohta M, Aikawa S, Komatsu M, Sawada T, Kagami Y, Morishima Y, et al. Development of novel humanized anti-CD20 antibodies based on affinity constant and epitope. Cancer Sci 2010; 101:201-209; PMID:19930155; http://dx.doi.org/10.1111/j.1349-7006.2009.01392.x
49. Fraker PJ, Speck JC, Jr. Protein and cell membrane iodinations with a sparingly soluble chloroamide, 1,3,4,6-tetrachloro-3a,6a-diphenylglycoluril. Biochem Biophys Res Commun 1978; 80:849-857; PMID:637870; http://dx.doi.org/10.1016/0006-291X(78)91322-0
50. Reiners C, Schneider R. Potassium iodide (KI) to block the thyroid from exposure to I-131: current questions and answers to be discussed. Radiat Environ Biophys 2013; 52:189-193; PMID:23475155; http://dx.doi.org/10.1007/s00411-013-0462-0
51. Wyffels L, De Bruyne S, Blanckaert P, Lambert DM, De Vos F. Radiosynthesis, *in vitro* and *in vivo* evaluation of 123I-labeled anandamide analogues for mapping brain FAAH. Bioorg Med Chem 2009; 17:49-56; PMID:19054678; http://dx.doi.org/10.1016/j.bmc.2008.11.019
52. Burvenich IJ, Schoonooghe S, Blanckaert P, Bacher K, Vervoort L, Coene E, Mertens N, De Vos F, Slegers G. Biodistribution and planar gamma camera imaging of ^{123}I- and ^{131}I-labeled $F(ab')_2$ and Fab fragments of monoclonal antibody 14C5 in nude mice bearing an A549 lung tumor. Nucl Med Biol 2007; 34:257-265; PMID:17383575; http://dx.doi.org/10.1016/j.nucmedbio.2006.12.006
53. Dias CR, Jeger S, Osso JA, Jr, Müller C, De Pasquale C, Hohn A, Waibel R, Schibli R. Radiolabeling of rituximab with (188)Re and (99m)Tc using the tricarbonyl technology. Nucl Med Biol 2011; 38:19-28; PMID:21220126; http://dx.doi.org/10.1016/j.nucmedbio.2010.05.010
54. Goldenberg DM, Juweid M, Dunn RM, Sharkey RM. Cancer imaging with radiolabeled antibodies: new advances with technetium-99m-labeled monoclonal antibody Fab' fragments, especially CEA-Scan and prospects for therapy. J Nucl Med Technol 1997; 25:18-23; quiz 34; PMID:9239599
55. Gratz S, Schipper ML, Dörner J, Höffken H, Becker W, Kaiser JW, Béhé M, Behr TM. LeukoScan for imaging infection in different clinical settings: a retrospective evaluation and extended review of the literature. Clin Nucl Med 2003; 28:267-276; PMID:12642703
56. Lamonica D, Czuczman M, Nabi H, Klippenstein D, Grossman Z. Radioimmunoscintigraphy (RIS) with bectumomab (Tc99m labeled IMMU-LL2, Lymphoscan) in the assessment of recurrent non-Hodgkin's lymphoma (NHL). Cancer Biother Radiopharm 2002; 17:689-697; PMID:12537673; http://dx.doi.org/10.1089/108497802320970307
57. Flanagan RJ, Jones AL. Fab antibody fragments: some applications in clinical toxicology. Drug Saf 2004; 27:1115-1133; PMID:15554746; http://dx.doi.org/10.2165/00002018-200427140-00004
58. Schmidt MM, Wittrup KD. A modeling analysis of the effects of molecular size and binding affinity on tumor targeting. Mol Cancer Ther 2009; 8:2861-2871; PMID:19825804; http://dx.doi.org/10.1158/1535-7163.MCT-09-0195
59. Wittrup KD, Thurber GM, Schmidt MM, Rhoden JJ. Practical theoretic guidance for the design of tumor-targeting agents. Methods Enzymol 2012; 503:255-268; PMID:22230572; http://dx.doi.org/10.1016/B978-0-12-396962-0.00010-0
60. Delgado C, Pedley RB, Herraez A, Boden R, Boden JA, Keep PA, Chester KA, Fisher D, Begent RH, Francis GE. Enhanced tumour specificity of an anti-carcinoembrionic antigen Fab' fragment by poly(ethylene glycol) (PEG) modification. Br J Cancer 1996; 73:175-182; PMID:8546903; http://dx.doi.org/10.1038/bjc.1996.32
61. Tolmachev V, Wallberg H, Andersson K, Wennborg A, Lundqvist H, Orlova A. The influence of Bz-DOTA and CHX-A″-DTPA on the biodistribution of ABD-fused anti-HER2 Affibody molecules: implications for ^{114m}In-mediated targeting therapy. Eur J Nucl Med Mol Imaging 2009; 36:1460-1468; PMID:19430786; http://dx.doi.org/10.1007/s00259-009-1134-9
62. Smith-Jones PM, Solit DB, Akhurst T, Afroze F, Rosen N, Larson SM. Imaging the pharmacodynamics of HER2 degradation in response to Hsp90 inhibitors. Nat Biotechnol 2004; 22:701-706; PMID:15133471; http://dx.doi.org/10.1038/nbt968
63. Olafsen T, Betting D, Kenanova VE, Salazar FB, Clarke P, Said J, Raubitschek AA, Timmerman JM, Wu AM. Recombinant anti-CD20 antibody fragments for small-animal PET imaging of B-cell lymphomas. J Nucl Med 2009; 50:1500-1508; PMID:19690034; http://dx.doi.org/10.2967/jnumed.108.060426
64. Olafsen T, Sirk SJ, Betting DJ, Kenanova VE, Bauer KB, Ladno W, Raubitschek AA, Timmerman JM, Wu AM. ImmunoPET imaging of B-cell lymphoma using 124I-anti-CD20 scFv dimers (diabodies). Protein Eng Des Sel 2010; 23:243-249; PMID:20053640; http://dx.doi.org/10.1093/protein/gzp081
65. Boswell CA, Marik J, Elowson MJ, Reyes NA, Ulufatu S, Bumbaca D, Yip V, Mundo EE, Majidy N, Van Hoy M, et al. Enhanced tumor retention of a radiohalogen label for site-specific modification of antibodies. J Med Chem 2013; 56:9418-9426; PMID:24131491; http://dx.doi.org/10.1021/jm401365h
66. König T, Skerra A. Use of an albumin-binding domain for the selective immobilisation of recombinant capture antibody fragments on ELISA plates. J Immunol Methods 1998; 218:73-83; PMID:9819124; http://dx.doi.org/10.1016/S0022-1759(98)00112-4
67. Skerra A. A general vector, pASK84, for cloning, bacterial production, and single-step purification of antibody Fab fragments. Gene 1994; 141:79-84; PMID:8163179; http://dx.doi.org/10.1016/0378-1119(94)90131-7
68. Skerra A. Use of the tetracycline promoter for the tightly regulated production of a murine antibody fragment in *Escherichia coli*. Gene 1994; 151:131-135; PMID:7828861; http://dx.doi.org/10.1016/0378-1119(94)90643-2
69. Schmidt TG, Skerra A. The *Strep*-tag system for one-step purification and high-affinity detection or capturing of proteins. Nat Protoc 2007; 2:1528-1535; PMID:17571060; http://dx.doi.org/10.1038/nprot.2007.209
70. Gill SC, von Hippel PH. Calculation of protein extinction coefficients from amino acid sequence data. Anal Biochem 1989; 182:319-326; PMID:2610349; http://dx.doi.org/10.1016/0003-2697(89)90602-7